Supplementary Information

Overshooting convection drives winter mixed layer under Antarctic sea ice

Ankit Bhadouriya[1,2,*], Bishakhdatta Gayen[2,3,**], Alberto C. Naveira Garabato[4], and Alessandro Silvano[4]

[1]Department of Mechanical Engineering, University of Melbourne, Melbourne, Australia
[2]Department of Aerospace Engineering, Indian Institute of Technology Kanpur, Kanpur, India
[3]Centre For Atmospheric and Oceanic Sciences, Indian Institute of Science, Bangalore, India
[4]Ocean and Earth Science, University of Southampton, Southampton, U.K.
[*]a.bhadouriya@unimelb.edu.au
[**]bishakhdatta.gayen@unimelb.edu.au

August 2022

Nature Communications

Supplementary Information Text

A. Maud Rise Mixed Layer

The water column at Maud Rise exhibits seasonal changes illustrated in Fig. 1, based on Argo float observations from 2015. In summer (Dec–Feb), near-surface waters are fresher due to sea ice melting and warmer due to solar radiation. In winter (Jun–Nov), near-surface waters are close to freezing and saltier due to sea ice formation. The figures demonstrate rapid mixed layer deepening in early winter, coinciding with substantial sea ice formation. Following this period, the deepening stabilizes as the mixed layer reaches thermodynamic equilibrium. Understanding the role of fine-scale convective turbulence in this seasonal mixed-layer evolution is crucial for predicting future sea ice volume distributions in a changing climate. The buoyancy frequency panel indicates that the weakest pycnocline stratification occurs in winter, facilitating the entrainment of deep waters into the mixed layer. This entrainment is primarily driven by the interaction between convective plumes and the pycnocline on small scales.

B. Large Eddy Simulation Model Details

The coupled LES model is driven by a seasonally varying atmospheric temperature, assumed to be in equilibrium with the snow surface temperature. We used climatological data from the ERA-5 atmospheric reanalysis to create an analytical function that forces the winter conditions in the model. Snow thickness is also included, as snow significantly reduces oceanic heat loss to the atmosphere due to its low thermal conductivity.

The model is initialized with idealized temperature and salinity profiles mimicking Argo float observations from early winter, typically averaged profiles from May (Fig. 2). These idealized profiles help elucidate key upper-ocean processes and ice-ocean interactions. A 100-meter sponge layer at the domain's bottom creates a non-reflective open ocean boundary.

Simulation results in Fig. 3 show the temporal evolution of laterally averaged water column properties, and indicate rapid mixed layer deepening during the first 40 days. As the mixed layer deepens, the mixed-layer temperature (MLT) increases due to warm water entrainment, and mixed-layer salinity (MLS) rises due to brine rejection and entrainment across the mixed-layer base. The density panel shows a significant decrease in pycnocline density difference from >0.2 kg/m^3 to <0.05 kg/m^3 over 120 days. The buoyancy frequency panel indicates reduced water column stratification throughout winter.

C. Comparison Between Different Regions Under Sea Ice

The primary difference between various sea ice-covered Southern Ocean regions resides in their salinity profiles and resulting water column stratification. Temperature gradients across the pycnocline have a modest effect on stratification, but can significantly influence the amount of heat entrained into the mixed layer. Fig. 4 shows the temperature and salinity profiles for the Maud Rise (red), Bellingshausen (green) and Ross Sea (blue) cases, used to initialize the simulations (solid lines). Buoyancy frequency profiles reveal that Maud Rise has the least stratified near-surface water column, while the Bellingshausen Sea has the most stratified upper ocean.

At the end of the simulation (light lines), after 130 days, the mixed layer has deepened by 50-60 m, and MLS has increased proportionally to sea ice formation. Maud Rise exhibits the largest increase in MLT, due to substantial entrainment of heat from the weak pycnocline. The reduction in pycnocline strength due to brine rejection is also significant at Maud Rise.

Fig. 5 shows that sea ice thickness is lowest at Maud Rise and highest in the Ross Sea case. The middle panels indicate nearly equal conductive heat flux across all regions. The bottom panel denotes a stark difference in ice-ocean interface heat flux, with Maud Rise displaying significantly higher values. This discrepancy is due to the greater MLT increase at Maud Rise (Fig. 6). The amount of deep, warm water entrainment into the mixed layer is contingent on water column stability, especially during the sea ice formation season. The primary difference in stability between Maud Rise and other areas is attributable to variations in MLS between the various regions (Fig. 6). The bottom panel of Fig. 6 shows MLD and changes in MLD for the three cases.

The variations in mixed-layer properties and dynamics due to sea ice formation result in different heat and salt fluxes at the mixed-layer base. Contour plots of heat fluxes for the three regions (Fig. 7, left panels) reveal significantly more heat entrainment into the mixed layer at Maud Rise compared to the other two areas. This is due to both the lower water column stability at Maud Rise, which allows greater penetration of convective saline plumes, and the larger heat content of the Maud Rise pycnocline, which

results in substantial upward eruptions of warm water. This also brings about enhanced salt fluxes at the mixed layer base (Fig. 7, right panels).

By evaluating each constituent of the turbulent temperature flux ($w'T'$) during the period of largest sea ice growth (model days 20 to 40), as shown in Fig. 8, we observe that w'_{rms} is nearly the same for all three cases under identical atmospheric forcing. However, the other component, T'_{rms}, differs between the areas. High values of T'_{rms} at Maud Rise highlight how the plume overshooting mechanism drives especially large upward heat entrainment as a result of the weak water column stability and relatively large pycnocline heat content there.

we compared the entrainment heat flux predicted using theoretical scaling with the heat flux measured at the mixed layer base from LES runs across various regions in Fig. 9. We specifically analyzed the temporal evolution of the vertical turbulent heat flux at the mixed layer base and contrasted it with the predicted heat flux derived from the formula $Q_b \approx C\Delta T w_{conv}$, where ΔT is the temperature difference between the plume penetration depth and the mixed layer base, and w_{conv} represents the convective velocity adjusted by a constant C. We established that the universal value of $C = 0.0015$ closely matches the simulated heat flux.

In our study, we evaluate the mixed layer properties beneath sea ice during periods of convective forcing in winter, employing theoretical scaling to assess changes and patterns over three consecutive years. We analyze three key variables: convective vertical velocity (w), which indicates the intensity of vertical mixing within the water column and is depicted for 2014, 2015, and 2016 in Fig. 10 top panels; buoyancy frequency (N), measuring the stability of the water column shown in Fig. 10 middle panels; and the temperature difference (ΔT) between the depth reached by the convective plume and the mixed layer depth, illustrated in Fig. 10 bottom panels. These variables, calculated for the month of June across the specified years, are correlated with the extent of sea ice observed in September of each respective year, providing insights into the interannual variability of sea ice and its underlying dynamics influenced by convective processes.

Supplementary Movies

Movie 1: Three-dimensional views of salinity, temperature and vertical velocity field help to show plume creation, interaction with the warm and salty pycnocline, and vertical motion, unveiling the detailed dynamics within the mixed layer.

Movie 2: Salty and cold plumes are created at the ice-ocean interface as a result of brine rejection. These plumes descend and overshoot the stratified, warm and salty pycnocline, leading to a complex rebound that causes entrainment.

Supplementary Figures

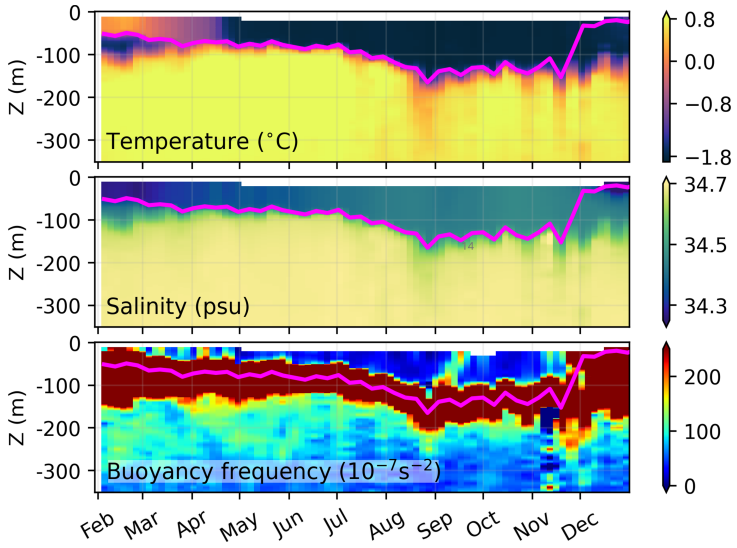

Supplementary Fig. 1: Dynamics of upper-ocean mixed layer in a high-latitude region heavily affected by sea ice. Seasonal evolution of the characteristic temperature, salinity and buoyancy frequency of the upper ocean over Maud Rise, measured by Argo floats. The mixed layer is indicated in all the panels by the magenta line.

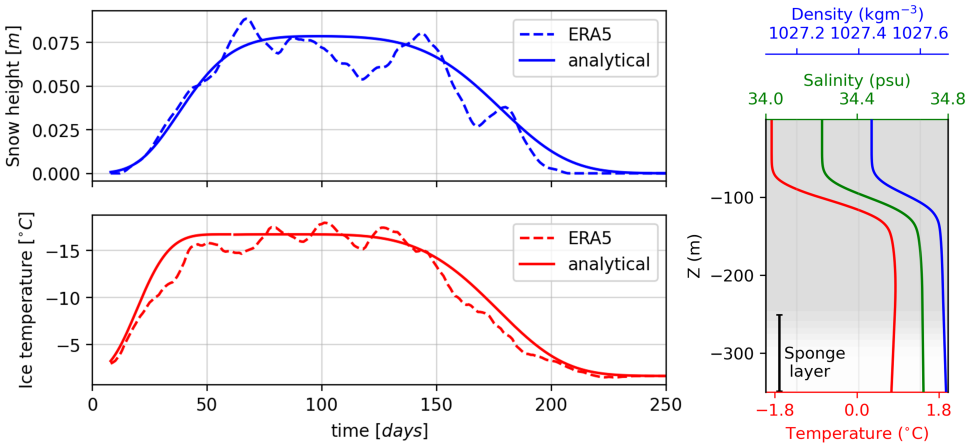

Supplementary Fig. 2: Boundary conditions and initial condition for the Maud Rise case. The left panel shows the temporal evolution of model input parameters: snow depth (top) and snow surface temperature (bottom). Each panel displays both climatological values from the ERA-5 atmospheric reanalysis and the analytical functions used to implement boundary conditions in the simulations. The right panel shows temperature, salinity and density profiles used as initial conditions. The bottom 150 m of the domain hosts a sponge layer, as indicated in the panel.

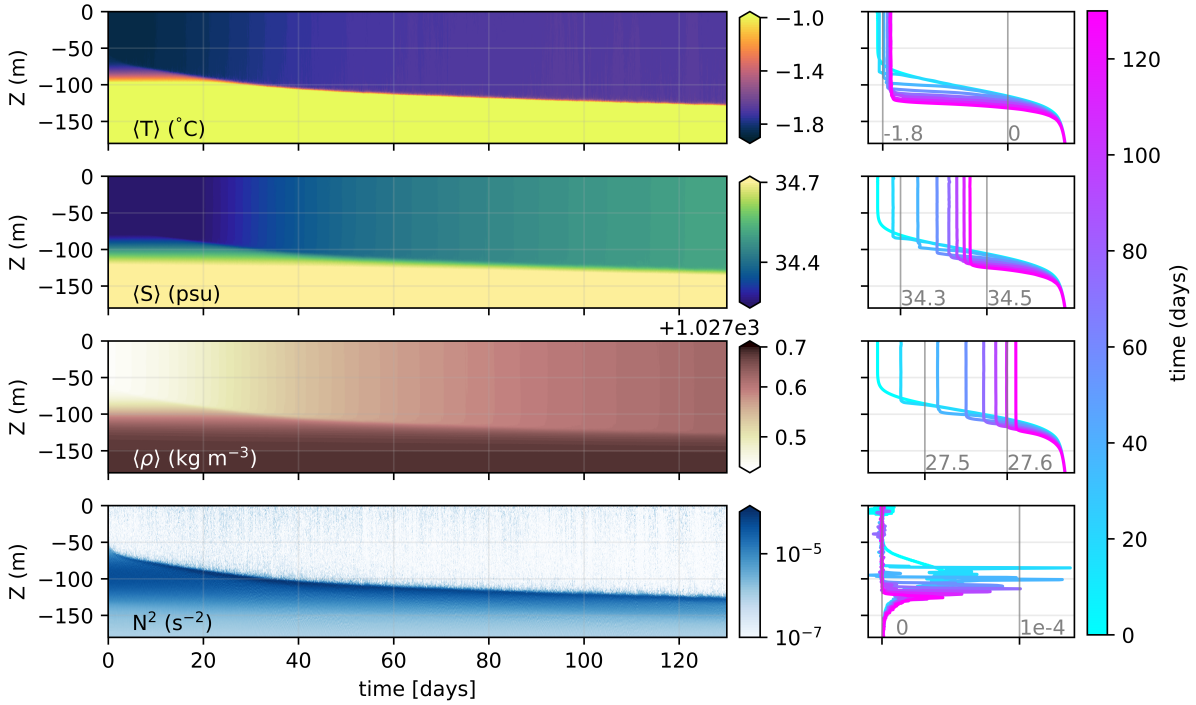

Supplementary Fig. 3: Mixed layer dynamics due to sea ice formation throughout winter. Contour plots in the left panels show the temporal evolution of simulated mixed layer properties, laterally averaged over the model domain: (a) temperature, (b) salinity, (c) density, and (d) buoyancy frequency. The panels reveal mixed layer deepening, warming, salinification and de-stratification as winter progresses. The right panels show line plots of how corresponding properties change with time.

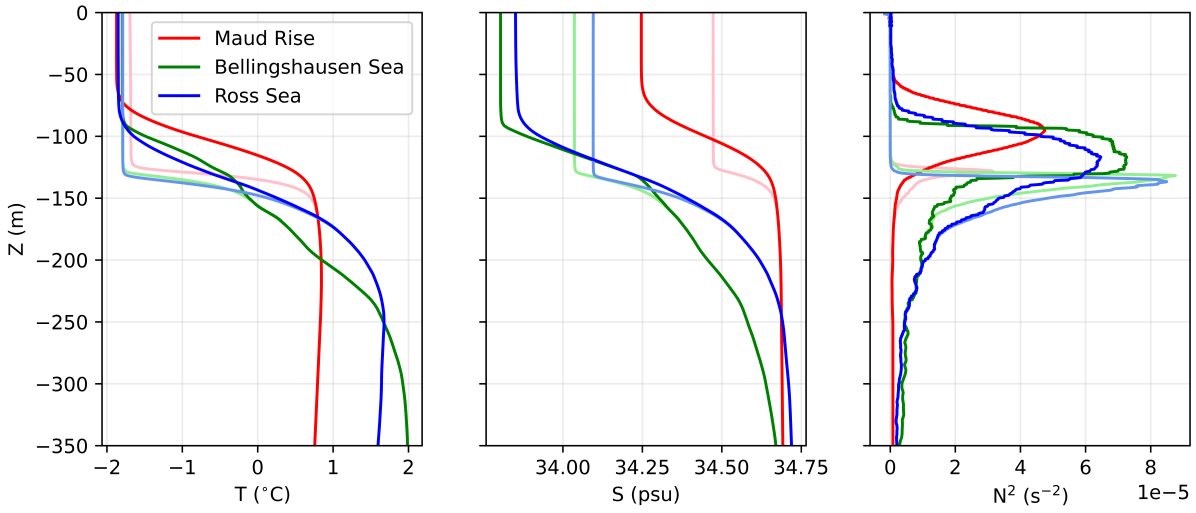

Supplementary Fig. 4: Water column profiles for different regions. Initial (bold lines) and final (light lines) simulated conditions for three areas: Maud Rise (red), Bellingshausen Sea (green), and Ross Sea (blue). The left panel shows temperature, the middle panel salinity, and the right panel buoyancy stratification.

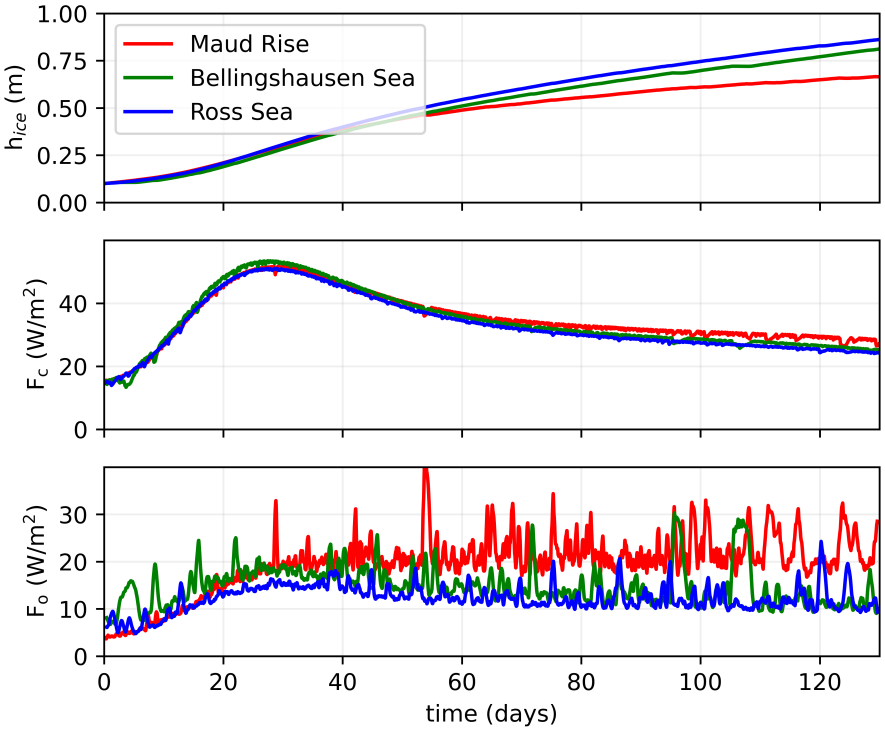

Supplementary Fig. 5: Sea ice thickness and interfacial heat fluxes throughout winter for different regions. Temporal evolution of simulated (a) sea ice thickness, (b) conductive heat flux, and (c) interfacial heat flux, averaged laterally over the model domain. The line colours are the same as in the previous figure.

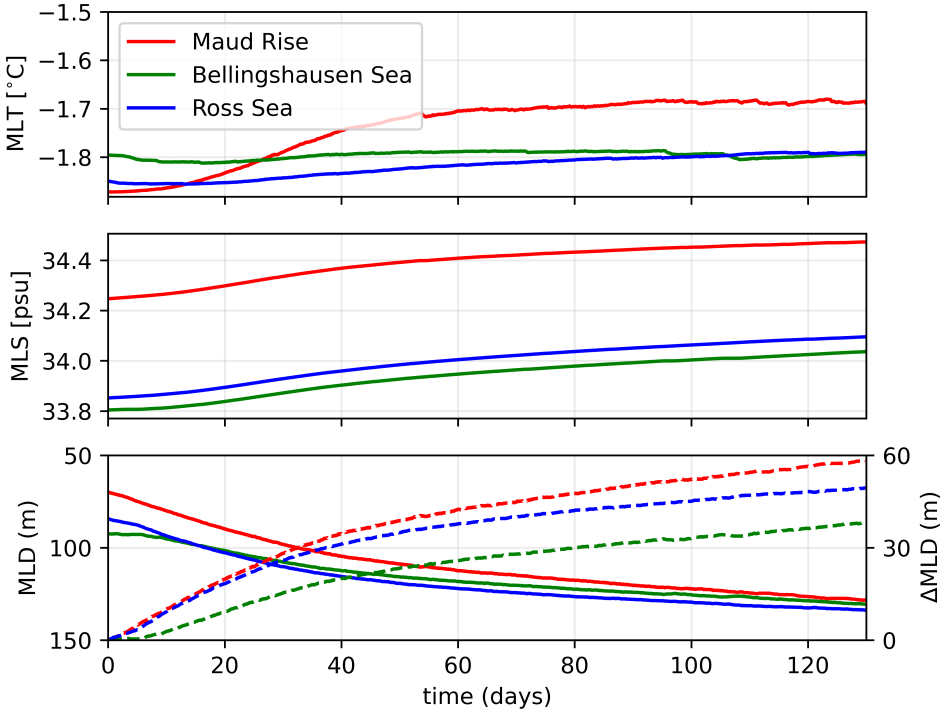

Supplementary Fig. 6: Mixed layer properties due to sea ice formation throughout winter for different regions. Temporal evolution of simulated mixed layer laterally-averaged properties: (a) temperature (MLT), (b) salinity (MLS), and (c) depth (MLD). The right vertical axis in (c) indicates a change in MLD from its initial values. The line colours are the same as in the previous figure.

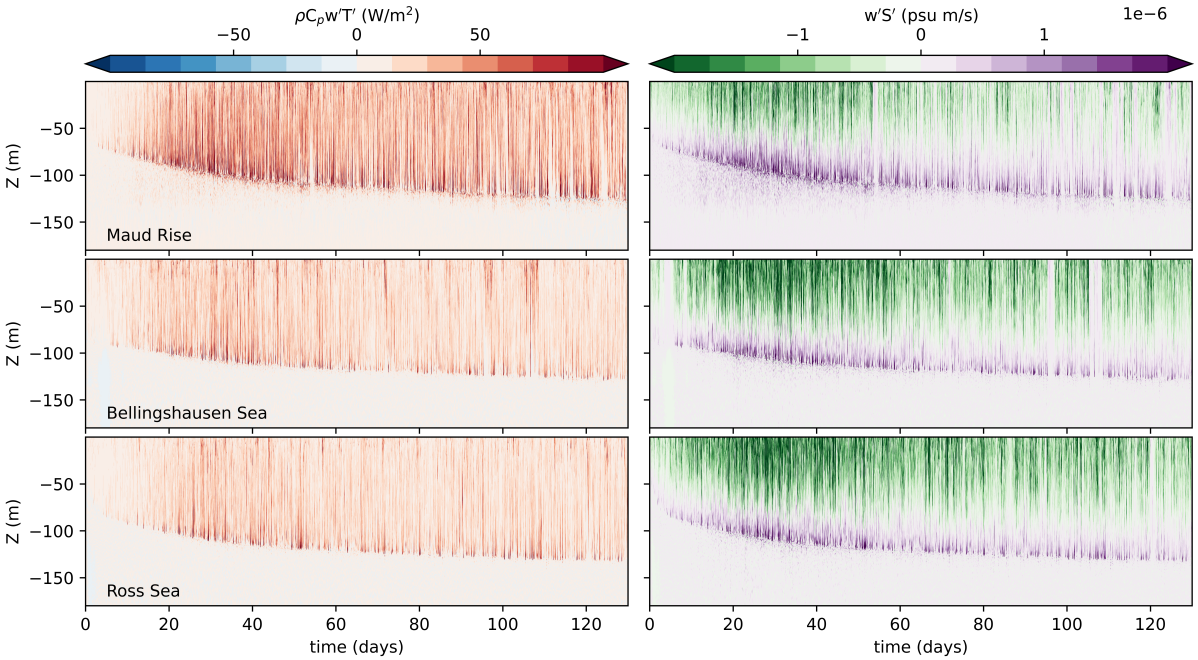

Supplementary Fig. 7: Turbulent fluxes due to mixed layer dynamics throughout winter for different regions. Temporal evolution of simulated laterally-averaged vertical turbulent heat flux (left panels) and vertical turbulent salinity flux (right panels) for the three areas. The panels show rapid mixed layer deepening for the Maud Rise and Ross Sea cases, compared to the Bellingshausen Sea scenario. The entrainment heat and salinity fluxes are highest for the Maud Rise.

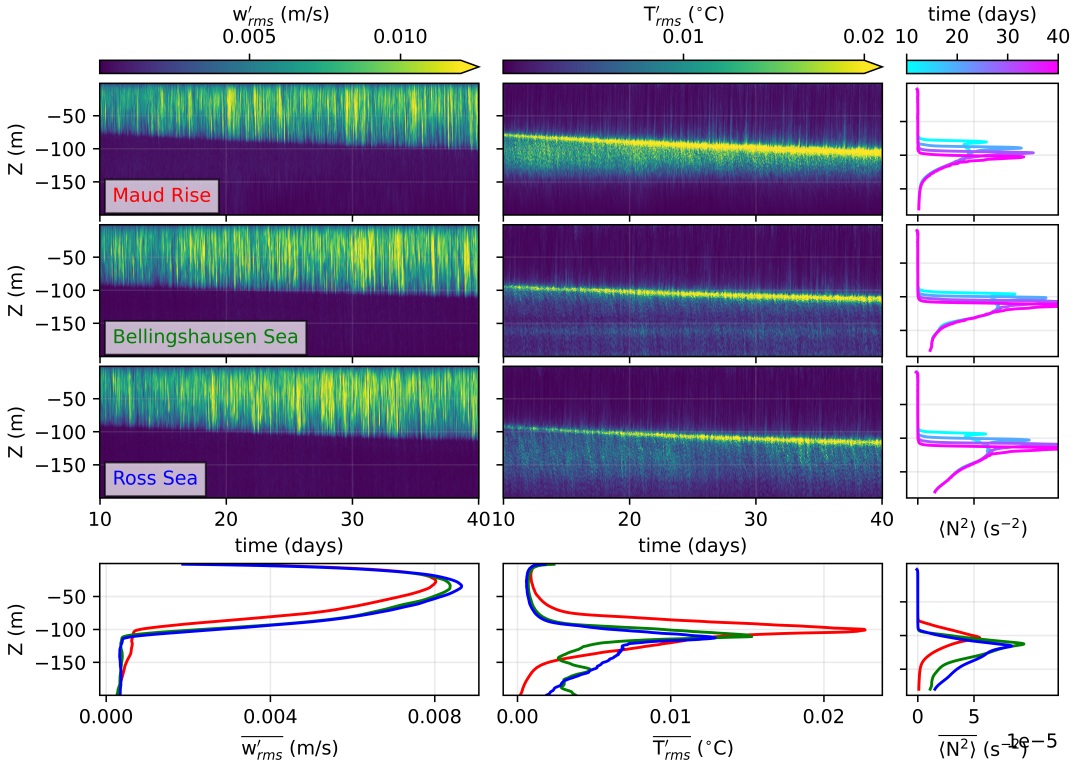

Supplementary Fig. 8: Variation during mixed layer deepening of the two fluctuating constituents of vertical turbulent heat flux ($w'T'$). The temporal evolution of fluctuating vertical velocity and temperature shows that the primary contribution to the turbulent vertical heat flux comes from temperature fluctuation, which makes heat flux different between the various areas. The bottom panels indicate temporally averaged quantities. The right-hand panels show line plots of buoyancy frequency changing over time.

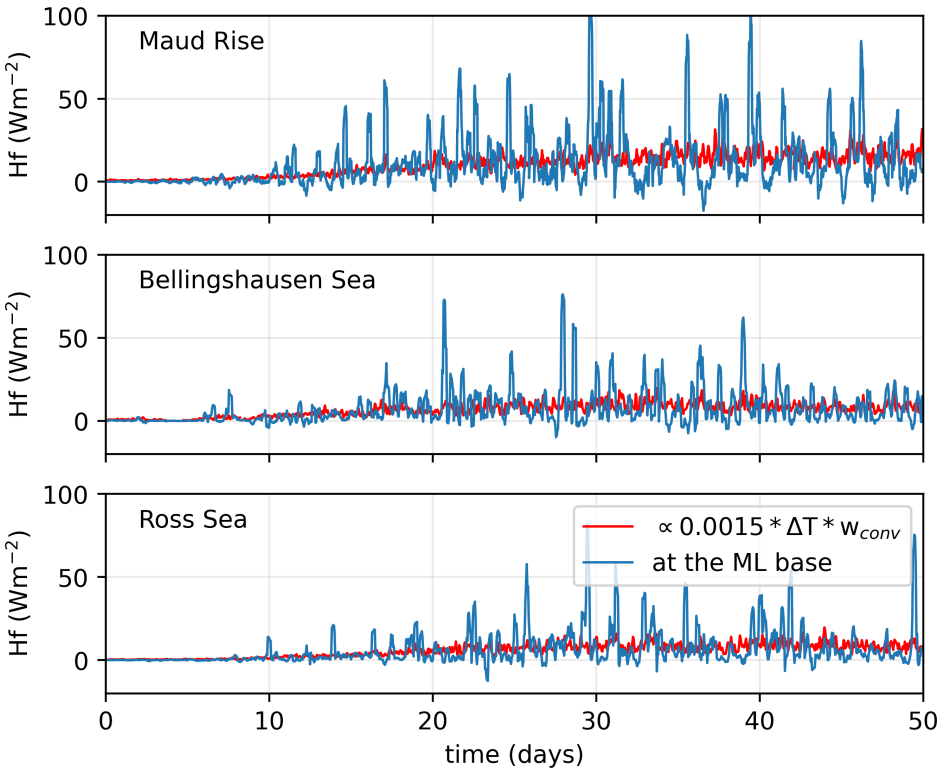

Supplementary Fig. 9: Entrainment heat flux predicted with the theoretical scaling compared with heat flux at the mixed layer base from LES for different regions. Temporal evolution of the vertical turbulent heat flux at the mixed layer base compared with the predicted heat flux based on $C * \Delta T * w_{conv}$, where ΔT is the difference in temperature between the plume penetration depth and the mixed layer base, and w_{conv} is the convective velocity multiplied by a constant C. The universal value of C=0.0015 was found to closely match the simulated heat flux. The theoretical estimate of the heat flux does not capture sharp peaks, due to a gross estimation of ΔT, which is based on an averaged mixed layer depth and the difference in temperature with respect to that depth.

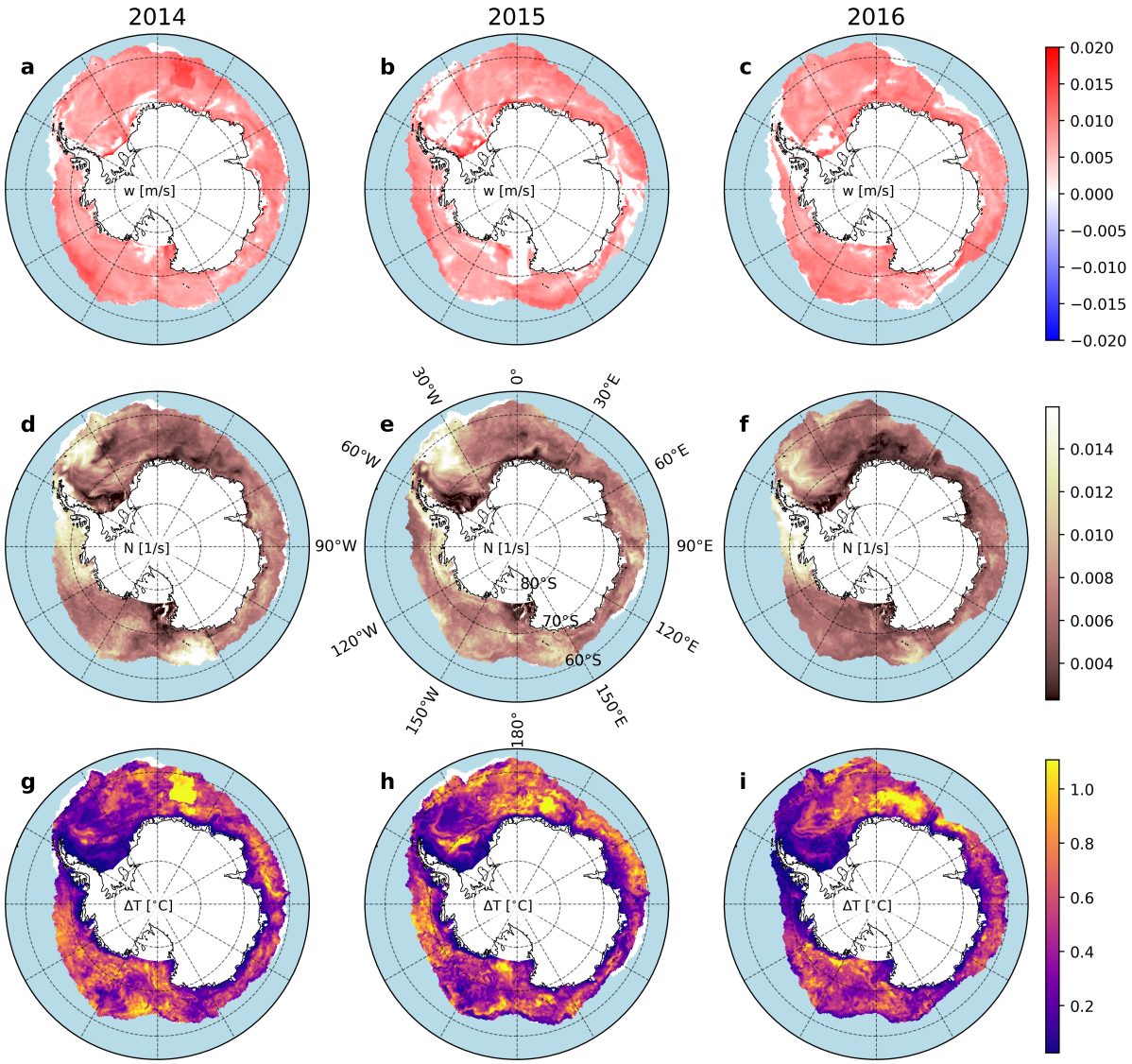

Supplementary Fig. 10: Evaluation of mixed layer properties under sea ice during convective forcing in winter using theoretical scaling. **a**–**c**: Convective vertical velocity (w). **d**–**f**: Buoyancy frequency, measuring the stability of the water column (N). **g**–**i**: Temperature difference (ΔT) between the depth of convective plume penetration and the mixed layer depth. Variables are calculated for the month of June in 2014 (left), 2015 (centre) and 2016 (right). Data in each figure corresponds to the extent of sea ice in September for the respective year.